Enabling passivity for Cartesian workspace restrictions

Hjorth, Sebastian; Lachner, Johannes; Ajoudani, Arash; Chrysostomou, Dimitrios

Published in:
2024 IEEE International Conference on Robotics and Automation (ICRA)

DOI (link to publication from Publisher):
10.1109/ICRA57147.2024.10610969

Publication date:
2024

Document Version
Accepted author manuscript, peer reviewed version

Enabling passivity for Cartesian workspace restrictions

Sebastian Hjorth[1], Johannes Lachner[2], Arash Ajoudani[3], and Dimitrios Chrysostomou[1]

***Abstract*— An emerging trend in the field of human-robot collaboration is the disassembly of end-of-life products. Safety is a crucial requirement of the disassembly process since worn-out or damaged products could break, possibly resulting in dangerous behavior of the robot. To protect the user from such behavior, this work addresses this challenge through the implementation of an energy-aware Cartesian impedance controller, combined with virtual workspace restrictions. Hereby, the passivity of the robotic system is ensured. The paper proposed two approaches to ensure the passivity of the system when subjected to workspace restrictions due to unplanned interactions and contact loss. The first approach employs an augmented energy tank with restricted energy flow. The second approach monitors the overall energy flow, regulating and separating non-passive behavior, caused by workspace restrictions. The approaches are evaluated and compared with each other, by using a KUKA LBR iiwa robot. The results highlight the potential of virtual workspace restrictions in human-robot collaborative disassembly tasks.**

I. Introduction

Over the past decade, the adoption of circular economy business models (CEBMs) across the various manufacturing sectors has been pushed by policymakers across Europe [1], [2]. However, the implementation of CEBMs poses the challenge of ensuring financial, environmental, and social viability, all of which rely on the efficiency of companies to recover and extract reusable resources and components from end-of-life products. As pointed out by [3], the process of disassembling and extracting components faces obstacles such as variability in part conditions, limited information about returned products, complex product structures, and increasing quality standards for recovered materials and components. These challenges can make it impossible to fully automate robotic systems to extract components, leading to the need for human-robot collaborative disassembly (HRCD) cells [4]. However, as shown in [5], there is a lack of physical human-robot interaction (pHRI) in HRCD cells as presented in [6]–[8].

Several potentially unexpected events and related safety concerns can arise during HRCD. One example is the sudden contact loss between components or gripper during component extraction. This poses injury risks to the human operator. Control strategies are therefore needed that enable pHRI [9]. One enabler are virtual walls to constraint the robot motion. This can shield the operator from potentially dangerous motions while still sharing the same workspace. An example setup for such an HCRD cell can be seen in Figure 1.

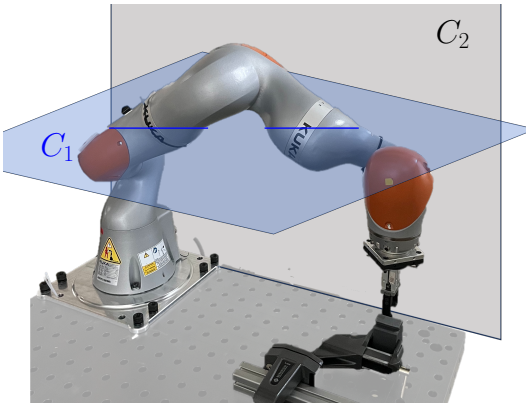

Fig. 1. Experimental setup for component extraction: a robot gripper extracts a component, simulated by a 3D-printed fixture, while being subject to virtual walls C_1 and C_2.

In addition to shielding the human from potentially dangerous behavior, ensuring that the human can physically interact with the robot in a safe manner is vital. In order to facilitate pHRI, it was formally proven in [10] that passivity-based control is needed.

Different control approaches have been proposed to restrict the robot's workspace virtually. The method proposed in [11] extends the Operational Space Control framework and enforces constraints by saturating the manipulator's Nullspace. In [12], an energy-aware impedance controller in combination with a repulsive potential field approach was presented to enforce virtual walls and joint space restrictions. However, both of these approaches did not investigate the influence of such constraints on the passivity of the robotic system.

The method presented in [13] proposes a passivity-based control approach for the motion planning of a 6-DOF robot in an obstacle populated environment; however, the robot could only adapt to forces applied to its end-effector. A passivity-based approach for kinematic control was proposed and verified in simulation in [14]. The approach was used for a kinematically redundant robot subjected to joint angle velocity limits. [15] investigated the use of control barrier functions to ensure the passivity of an artificial potential field method to avoid obstacles. A passivity-based control approach for singularity handling was proposed in [16]. The approach is based on control barrier functions and was validated in simulation for a 7-DOF robot. Another control-

[1]Dept. of Materials and Production, Aalborg University, Aalborg, Denmark. sshj@mp.aau.dk

[2] Department of Mechanical Engineering, Massachusetts Institute of Technology, Cambridge, USA.

[3] Istituto Italiano di Tecnologia, Genoa, Italy.

This work was supported by

barrier function approach to enforce virtual walls for an impedance controller was presented in [17].

As pointed out in [18], it is vital to monitor and restrict the amount of energy allowed to be stored and injected by the controller into the robot to ensure the passivity and safety of the system. Passivity becomes even more critical when it comes to kinematically redundant robots, e.g., when joints are subject to virtual walls that move in the nullspace of the task Jacobian. This can yield to an abrupt rise in the system energy, leading to the system's instability.

In this work, we aim to handle this behavior whilst enabling safe pHRI by combining the energy-aware Cartesian impedance controller presented in [19] with the method presented in [12] to enforce virtual workspace restrictions. Additionally, the work presented in [12] is extended by investigating two approaches for ensuring the passivity of the system and comparing their performance to each other based on a faulty proof-of-concept disassembly task. In summary, the main contributions of this work are as follows:

- Investigation of the passivity-related behavior associated to virtual walls.
- Presenting two control approaches to ensure the passivity of the system when subject to virtual walls.
- An experimental comparison between the proposed control strategies on a kinematically redundant robot in a proof-of-concept faulty component extraction experiment.

The remainder of the paper is structured as follows: In section II, the energy flow of the virtual walls and theory of the two implemented passivity-based methods are presented. In section III, the experimental results are shown while section IV summarizes and discusses the findings of the experimental results. In section V, future research directions are presented.

II. Methods

Notation: Vectors and matrices are indicated by small and capital bold letters, respectively. The transpose of $\mathbf{s}$ is represented as $\mathbf{s}^\top$. The wrench of frame c in respect to frame j expressed in i is indicated by $\mathbf{w}_c^{i,j}$.

A. Control approach

The control torques $\boldsymbol{\tau}_{\text{Imp}}^\top \in \mathbb{R}^n$ can be expressed as the sum of torques associated with the Cartesian springs $\boldsymbol{\tau}_{\text{Spring}}^\top \in \mathbb{R}^n$ and the torques for virtual dissipation $\boldsymbol{\tau}_{\text{Damp}}^\top \in \mathbb{R}^n$:

$$\boldsymbol{\tau}_{\text{Imp}}^\top = \boldsymbol{\tau}_{\text{Spring}}^\top - \boldsymbol{\tau}_{\text{Damp}}^\top. \tag{1}$$

The Cartesian springs are placed between infinitesimal body twist displacements $\Delta\boldsymbol{\eta} \in se(3)$. The diagonal rotational and translational stiffness matrices are denoted $\mathbf{K}_r \in \mathbb{R}^{3\times3}$ and $\mathbf{K}_t \in \mathbb{R}^{3\times3}$, respectively; The coupling between rotational and translational terms is described by the matrix $\mathbf{K}_c \in \mathbb{R}^{3\times3}$. The motion generating elastic wrench is:

$$se^*(3) \ni \mathbf{w}_K^{\text{EE,EE}\top} = \begin{bmatrix} \mathbf{K}_t & \mathbf{K}_c \\ \mathbf{K}_c^\top & \mathbf{K}_r \end{bmatrix} \Delta\boldsymbol{\eta}. \tag{2}$$

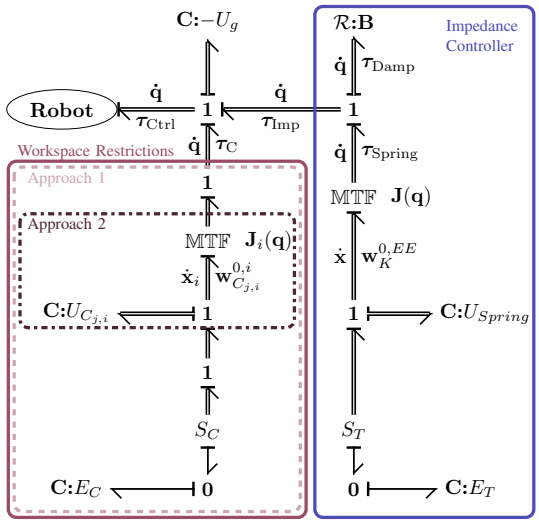

Fig. 2. Bond graph representation, depicting the interconnection of the robot, the impedance controller, and controller to enable virtual workspace restrictions.

The elastic wrench, expressed in spatial coordinates 0, can be derived by $\mathbf{w}_K^{0,\text{EE}\top} = \mathbf{Ad}_{\mathbf{H}_0^{\text{EE}}}^\top \mathbf{w}_K^{\text{EE,EE}\top}$, with $\mathbf{Ad}_{\mathbf{H}_0^{\text{EE}}}^\top \in \mathbb{R}^{6\times6}$ being the Adjoint Transformation [20]. The motion generating torques $\boldsymbol{\tau}_{\text{Spring}}^\top \in \mathbb{R}^n$ can then be mapped onto the joint space by the Spatial Jacobian $\mathbf{J}(\mathbf{q})$ as follows:

$$\boldsymbol{\tau}_{\text{Spring}}^\top = \mathbf{J}(\mathbf{q})\mathbf{w}_{\text{K}}^{0,\text{EE}\top}. \tag{3}$$

The dissipation torques can be calculated with the damping matrix $\mathbf{B} \in \mathbb{R}^{n\times n}$ and the joint velocities $\dot{\mathbf{q}} \in \mathbb{R}^n$ as

$$\boldsymbol{\tau}_{\text{Damp}}^\top = \mathbf{B}(\mathbf{q})\ \dot{\mathbf{q}}. \tag{4}$$

More details about the calculation of $\boldsymbol{\tau}_{\text{Imp}}^\top$ can be found in [19].

B. Energy flow of virtual walls

The energy stored in an impedance-controlled robot can be described as the sum of the storage function $S_{\text{Ctrl}} \in \mathbb{R}$ of the controller and the storage function $S_{\text{Rob}} \in \mathbb{R}$ of the robot: $S = S_{\text{Ctrl}} + S_{\text{Rob}} \in \mathbb{R}$ ([21]). As shown in [10], S_{Rob} is physically bounded and therefore the robot related to S_{Rob} is passive. Hence, the controlled robotic system is only passive if the controller, described by S_{Ctrl}, is passive. It is possible to express S_{Ctrl} as:

$$S_{\text{Ctrl}} = U_{\text{Ctrl}} - U_{\text{gravity}} \in \mathbb{R} \tag{5}$$

For simplicity, we will neglect U_{gravity} in the remainder of the paper and presume it is compensated in an energy consistent way. Throughout this work, we will use the bond graph representation in Figure 2 to visualize the storage functions and energy flows (including their directions). More details about Bond Graphs can be found in [22].

The energy flow of the controller can be described by the rate of change of S_{Ctrl}, denoted as $P_{\text{Ctrl}} \in \mathbb{R}$. P_{Ctrl} is the sum of the energy flows through the ports $(\boldsymbol{\tau}_{\text{Imp}}, \dot{\mathbf{q}})$ (impedance controller) and $(\boldsymbol{\tau}_C, \dot{\mathbf{q}})$ (workspace restriction). These energy

flows will be denoted $P_{\text{Imp}} \in \mathbb{R}$ and $P_{\text{C}} \in \mathbb{R}$, respectively. They are related to P_{Ctrl} by:

$$P_{\text{Ctrl}} + P_{\text{Imp}} + P_{\text{C}} = 0 \tag{6}$$

This equation can be expanded into its sub-components resulting in,

$$P_{\text{Ctrl}} + \underbrace{\underbrace{P_{\text{Spring}}}_{\boldsymbol{\tau}_{\text{Spring}}\dot{\mathbf{q}}} + \underbrace{P_{\text{Damp}}}_{\boldsymbol{\tau}_{\text{Damp}}\dot{\mathbf{q}}}}_{\boldsymbol{\tau}_{\text{Imp}}\dot{\mathbf{q}}} + \underbrace{P_{\text{C}}}_{\boldsymbol{\tau}_{\text{C}}\dot{\mathbf{q}}} = 0. \tag{7}$$

As shown in [19], the control action of the energy-aware impedance controller is passive. Hence, possible non-passive behavior originates from the energy injected by the control action of the virtual walls. This will be the focus of the remainder of the paper (left part of Figure 2).

In the event of an external disturbance the robot's link i moves towards a virtual Cartesian workspace restriction $C_j \cong \mathbb{R}^3$ and enters the activation distance $d_{i,C_j} \in \mathbb{R}$ at which the virtual Cartesian workspace restriction starts to introduce a repelling wrench $\mathbf{w}_{C_j}^{0,i\,\top} \in se^*(3)$ on the respective link. This wrench increases exponentially as it comes closer to the limit of the virtual wall and slows down the motion of the link. Hence, the kinetic energy of the link is reduced through virtual dissipation. The moment in which the link's motion towards the virtual workspace restriction comes to a hold, no energy flows between the workspace restriction and the robot's link as the link's velocity is zero. When the robot's link is repelled by $\mathbf{w}_{C_j}^{0,i\,\top}$ away from the virtual workspace restriction, energy is injected into the system, resulting in an acceleration of the link in the opposite direction of the virtual wall. In the event that the energy injected by the virtual wall P_C is greater than the energy dissipated by P_{Damp}, the system becomes non-passive. This can result in the instability of the system.

Two approaches will be presented and investigated. The first approach (subsection II-C) utilizes the concept of an augmented energy tank. The second approach (subsection II-D) monitors the overall energy flow of the system and decouples non-passive control actions from the constraint if necessary. This is done without the need of an energy tank.

C. Approach 1: Separate Energy Tank

In approach 1, a second energy tank E_C is introduced, next to the one that stores the energy in E_T to enable passivity of the Cartesian impedance controller (Figure 2). Both energy tanks have their individual energy flow, which can be regulated such that the energy flow of the main task does not restrict the energy flow of the virtual walls. The overall allocated energies for the task (E_T) and the workspace constraints (E_C) are separated. This is especially important if links which are subject to workspace constraints do not influence the main task. Otherwise, this could lead to draining of E_T and therefore a loss of the task. Another scenario could be that the energy flow due to the virtual walls always refills E_T, even during a non-passive task action. Hence, based on the definition of P_{Ctrl} at $(\boldsymbol{\tau}_{\text{Ctrl}}, \dot{\mathbf{q}})$ and definition of P_{Damp} in (7), it can be seen that any increase of energy S_{Ctrl} is due to a negative energy flow of the power P_T and P_C:

$$-\big(P_T + P_C\big) \geq P_{\text{Ctrl}}. \tag{8}$$

Here, P_C can be calculated by taking into account all virtual walls C_j and restricted links i. It can be calculated by: $P_C = \sum_j \sum_i P_{C_{j,i}}$. In general, multiple links can encounter the same virtual wall and one link can encounter multiple virtual walls. We will use the same notation for i and j for the remainder of the paper.

We can bound the controlled robots energy (storage function S), by bounding S_{Ctrl}. This can be implemented by the aforementioned virtual energy tanks E_T and E_C, which are individually bounded by their respective upper and lower bound $\overline{E}_T/\underline{E}_T$ and $\overline{E}_{\text{C}}/\underline{E}_C$. The individual energy flows of the tanks are denoted as $\dot{E}_C$ and $\dot{E}_T$. The implementation of these energy tanks alters the energy flow of the system such that

$$P_{\text{Ctrl}} + \dot{E}_T + \dot{E}_C \leq 0 \tag{9}$$

holds true where

$$\dot{E}_{\text{T}} = -P_T \quad \text{and} \quad \dot{E}_C = -P_C. \tag{10}$$

Note, that the passivity violating directions of $\dot{E}_C$ and P_{Ctrl} at $(\boldsymbol{\tau}_{\text{C}}, \dot{\mathbf{q}})$ are in opposite directions. In a first step, we will ensure that the energy tank stays within its upper and lower limits $\overline{E}_{\text{C}}$ and $\underline{E}_{\text{C}}$ through the following two variables $h \in \mathbb{R}$ and $l \in \mathbb{R}$.

$$\begin{aligned} h &= \begin{cases} 0 & \text{if } \dot{E}_C \geq 0 \wedge E_{\text{C}} \geq \overline{E}_{\text{C}} \\ 1 & \text{otherwise} \end{cases} \\ l &= \begin{cases} 0 & \text{if } \dot{E}_C \leq 0 \wedge E_{\text{C}} \leq \underline{E}_{\text{C}} \\ 1 & \text{otherwise} \end{cases} \end{aligned} \tag{11}$$

In a second step, negative values of P_C are restricted to the predefined limit $\underline{\dot{E}}_C$ through the scaling factor

$$\alpha = \begin{cases} \frac{\underline{\dot{E}}_C}{\dot{E}_C} & \text{if } \dot{E}_C < \underline{\dot{E}}_C \leq 0 \wedge l = 1 \\ 1 & \text{otherwise.} \end{cases} \tag{12}$$

Based on these augmentations, the energy flow $\dot{E}_C$ can be rewritten as

$$\dot{E}_C = \begin{cases} \alpha l \dot{E}_C & \text{if } \dot{E}_C \leq 0 \\ h \dot{E}_C & \text{otherwise.} \end{cases} \tag{13}$$

To limit the rate of energy that can be drained from the tank by P_C, the scaling factor α has to be applied to the resulting torques $\boldsymbol{\tau}_C^\top$ in the following way:

$$\boldsymbol{\tau}_C^\top = \alpha l \sum_i \sum_j \mathbf{J}_i^\top(\mathbf{q}) \mathbf{w}_{C_j}^{0,\text{i}\,\top} \tag{14}$$

D. Approach 2: Flow limiting

For this method, no separate energy tank is introduced (subsection II-C). Instead, this method employs an energy flow regulation method and a power-based decoupling strategy for handling passivity-violating behavior introduced by a specific virtual wall. As in the previous method, the amount of energy flow of the control actions is restricted. However, since there is no additional energy tank for this method, the energy flow of the workspace restrictions is now regulated at the port $(\boldsymbol{\tau}_C, \dot{\mathbf{q}})$, instead of at the E_C (Figure 2). The overall energy flow P_Ctrl at power port $(\boldsymbol{\tau}_\mathrm{Ctrl}, \dot{\mathbf{q}})$ is monitored. In case $P_\mathrm{Ctrl} > 0$, the method identifies the passivity-violating action (virtual wall and respective link) and decouples it from P_Ctrl. Instead of monitoring the energy flow of the tank ($\dot{E}_C < 0$), this method restricts P_C in a positive direction. Based on P_C and a chosen upper limit $\overline{P}_C$, the energy flow restriction variable $\alpha \in \mathbb{R}$ for the virtual walls is calculated by:

$$\alpha = \begin{cases} \frac{\overline{P}_C}{P_C} & \text{if } P_C > \overline{P}_C \geq 0 \\ 1 & \text{otherwise.} \end{cases} \tag{15}$$

This variable scales the resulting torques $\boldsymbol{\tau}_C^\top$ which are defined as the sum of all torques generated by the repelling wrenches of all virtual walls:

$$\boldsymbol{\tau}_{C,\alpha}^\top = \alpha \sum_i \sum_j \mathbf{J}_i{}^\top(\mathbf{q}) \mathbf{w}_{C_{j,i}}^{0,\mathrm{i}}{}^\top. \tag{16}$$

Based on these torques, the restricted energy flow at the power port $(\boldsymbol{\tau}_C, \dot{\mathbf{q}})$ can be expressed as $P_C^\dagger = \alpha \sum_j \sum_i P_{C_{j,i}} \in \mathbb{R}$. Even though the injected energy flow is already restricted through α, it is still possible to violate the passivity of the system. In the next step, the overall energy flow P_Ctrl at the power port $(\boldsymbol{\tau}_\mathrm{Ctrl}, \dot{\mathbf{q}})$ is calculated and monitored as follows:

$$P_\mathrm{Ctrl} = (\boldsymbol{\tau}_\mathrm{Imp}^\top + \boldsymbol{\tau}_{C,\alpha}^\top)\dot{\mathbf{q}}. \tag{17}$$

In case $P_\mathrm{Ctrl} > 0$, the robotic system becomes non-passive. Since the Impedance Controller is passive, this non-passivity must arise through the actions of the workspace restrictions. Hence, the energy flows $P_{C_{j,i}}$ are individually checked if they contributed to the non-passivity of the system. In case $P_{C_{j,i}} > 0$, they are decoupled through the variable $\phi_{j,i}$:

$$\phi_{j,i} = \begin{cases} 0 & \text{if } P_\mathrm{Ctrl} > 0 \wedge P_{C_{j,i}} > 0 \\ 1 & \text{otherwise.} \end{cases} \tag{18}$$

Consequently, the energy flow at the port $(\boldsymbol{\tau}_\mathrm{Ctrl}, \dot{\mathbf{q}})$ can be rewritten to:

$$P_\mathrm{Ctrl} + P_\mathrm{Imp} + \underbrace{\alpha \sum_i \sum_j \phi_{j,i} P_{C_{j,i}}}_{P_C^\dagger} = 0. \tag{19}$$

Finally, this method is implemented by scaling the repelling wrenches $\boldsymbol{\tau}_C^\top$ by the scaling factor α and the decoupling variable $\phi_{j,i}$:

$$\boldsymbol{\tau}_C^\top = \alpha \sum_i \sum_j \phi_{j,i} \mathbf{J}_i{}^\top(\mathbf{q}) \mathbf{w}_{C_{j,i}}^{0,\mathrm{i}}{}^\top \tag{20}$$

III. Experiments & Results

The above-presented approaches were tested in a proof-of-concept component extraction experiment. The setup consists of a KUKA LBR iiwa 7 robot, equipped with a pneumatic gripper and a 3D-printed fixture (Figure 1). The robot is controlled via an external PC and KUKA's Fast-Research-Interface. The robot model was created with the *Exp[licit]*-library[1].

The general concept of the experimental setup is to simulate an accidental contact loss during a separation process of two components whilst a human operator is in close proximity to the robot. This scenario aims to showcase the possibility of enabling close collaboration during HRCD tasks. The experiments can be divided into two different phases: 1) accidental phase; and 2) pHRI-phase. 1) Accidental phase : The presented use-case assumes that the position of the component is known a priori. Hence, the accidental phase (highlighted in green) starts with the gripper already grasping the fixture. While moving the desired pose along the TCP z-axis, the controller begins to increase the pulling force along its until it reaches a scalar set force $\mathbf{f}_\mathrm{extract,z}$. When $\mathbf{w}_{ext,z}^{0,EE} = \mathbf{f}_\mathrm{extract,z}$, the gripper is triggered externally to open, simulating the failure of the part. To keep the robot in a predefined workspace, the robot's 6^th-link will encounter the virtual wall C_1 (Figure 1). This virtual wall is set to avoid collisions with the human co-worker if a failure happens. The accidental phase is concluded as soon as the robot TCP has reached its nominal pose. 2) pHRI-phase: During pHRI, the robot's 6^th-link and 4^th-link were manually pushed into the virtual walls C_1, C_2, respectively. Excessive forces were exerted, to test a worst-case scenarios during pHRI. Additionally, the links were kept in contact with the virtual walls for a longer time, to validate the robot robot stability when additional energy is injected while going in and out the virtual walls (section II).

As mentioned in section I, the energy-aware impedance controller of [19] is utilized for the task. In order to showcase that its control action is passive, the corresponding energy tank E_T will be plotted for both experiments. For a more detailed description on how passivity is achieved, the reader is referred to [19]. The control parameters for both control approach are shown in Table Iand an video of the experiments can be found in https://youtu.be/wzOtvGffonY.

A. Approach 1: Separate Energy Tank

This subsection will show the benefits of approach 1 by referring to Figure 3. When the gripper released the fixture in the accidental phase ($4 - 12$ s, highlighted in green), the stored potential energy U_Spring accelerated the end-effector abruptly towards $\mathbf{H}_d^0$. The sudden release of energy caused the end-effector to surpass $\mathbf{H}_d^0$, and consequently, the 6^th-link entered the activation area of C_1 (d_{6,C_1} crossed the dashed line). As soon as the 6^th-link passed the activation distance, the repelling wrench $\mathbf{w}_{C_{1,6}}^{0,6}$ increased and the link's

[1] https://explicit-robotics.github.io/

TABLE I

CONTROL PARAMETERS USED DURING THE DIFFERENT EXPERIMENTS.

Energy-Aware Impedance controller [19]		
Translational spring stiffness	$\mathbf{K}_t$	$800 \cdot \mathbf{I}_3$
Rotational spring stiffness	$\mathbf{K}_r$	$200 \cdot \mathbf{I}_3$
Coupling spring stiffness	$\mathbf{K}_c$	$0 \cdot \mathbf{I}_3$
Max. allowed energy	$\overline{E}_{\text{total}}$	2J
Max. allowed power	$\overline{P}_{\text{motion}}$	0.5W
Initial damping	$\mathbf{B}$	$5 \cdot \mathbf{I}_7$
Extraction force	$\mathbf{f}_{\text{pull,z}}$	62N
Virtual walls [12]		
Translational spring stiffness	$\mathbf{L}_{C_j,\mathrm{t}_i}$	$10 \cdot \mathbf{I}_3$
Activation distance	$d_{0,C_{1/2}}$	0.07m
Field potential	γ	2
Approach 1: Control parameters		
Max. allowed power to be injected	$\underline{\dot{E}}_{\text{C}}$	-0.175W
Max. Energy level in the tank	$\overline{E}_{\text{C}}$	20J
Min. Energy level in the tank	$\underline{E}_{\text{C}}$	0.5J
Initial Energy level in the tank	E_{C}	15J
Approach 2: Control parameters		
Max. allowed power to be injected	P_{C}	-0.25W

kinetic energy was virtually dissipated ($\sim$ 14.75 s). This resulted in a positive energy flow $\dot{E}_C$ at the port of the energy tank E_C, which increased the level in E_C ($\dot{E}_C$-plot, magnified in purple window). When link 6 reached its maximal penetration, it was pushed out of the activation distance by $\mathbf{w}^{0,6}_{C_{1,6}}$. It can be seen that the energy flow out of the tank ($\dot{E}_C < 0$) did not violate the limit $\underline{\dot{E}}_C$ and the injected energy remained approximately constant (E_C-plot, magnified in the purple window). Consequently, the energy injected by the control action C_1 did not violate the passivity of the system during the accidental phase. After the end-effector had reached its desired pose, the pHRI-phase started ($\sim$ 15.5 s, highlighted in red). The robot's 6$^{\text{th}}$-link was manually pushed into the virtual wall C_1 at $16.2-18$ s and again at $23-26.2$ s. Following the same procedure, the robot's 4$^{\text{th}}$-link was manually pushed into the virtual wall C_2 ($\sim 20-22$ s). When observing the energy flow $\dot{E}_C$ more closely, a similar behavior as in the accidental phase can be observed when either link 4 or 6 enter the activation distance of a virtual wall (dashed line): The amount energy stored in E_{C} and the repelling wrenches $\mathbf{w}^{0,6}_{C_{1,6}}$/$\mathbf{w}^{0,4}_{C_{2,4}}$ increased and decreased again as the links exited the activation distance of the respective constraint. Additionally, it can be seen that when the links were held within the activation distance of a virtual wall, $\dot{E}_C$ changed direction at a high frequency. This behavior occurred since the repelling wrenches of the respective virtual walls were nearly equal to the externally applied wrenches. However, due to the high repelling forces of the virtual walls (max. $\mathbf{w}^{0,6}_{\text{ext,z}} = -40$ N, max.$\mathbf{w}^{0,4}_{\text{ext,x}} = 60$ N), even minor fluctuations in the externally applied wrenches lead to changes in the direction of $\dot{E}_C$. If left unchecked, the oscillations in $\dot{E}_C$ could result in instabilities (section II) since all the accumulated energy in E_C could be released in a single time instant. When the robot's 6$^{\text{th}}$-link was manually pushed into C_1 for the first time ($\dot{E}_C$,

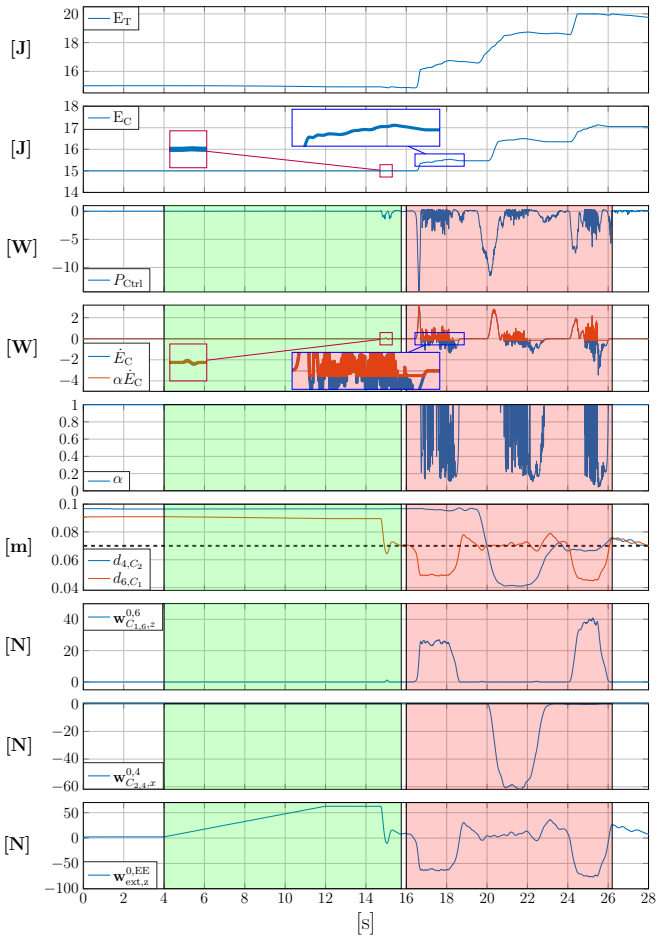

Fig. 3. Observable quantities of approach 1: Energy tanks E_T, and E_C; unrestricted and by α restricted energy flow $\dot{E}_C$; repelling wrenches $\mathbf{w}^{0,6}_{C_{1,6},z}$ and $\mathbf{w}^{0,4}_{C_{2,4},x}$ of virtual walls C_1 and C_2 along their repelling direction; external wrench acting along the TCP's z-axis, $\mathbf{w}^{0,EE}_{ext,z}$.

magnified in the blue window), it can be seen how $\dot{E}_C$ initially got scaled by α and limited to the maximal allowed energy flow $\underline{\dot{E}}_C$. Moreover, while exiting the activation distance of the respective virtual wall, only a fraction of the stored energy E_C was injected back into the system. This shows the benefit of the introduced energy flow limitation (subsection II-C): The level in E_C rises at a higher rate than it can be drained and therefore the system stays passive even during high-frequent changes in $\dot{E}_C$. Additionally, it can be seen that even though the amount of energy transfer through port ($\boldsymbol{\tau}_C$,$\dot{\mathbf{q}}$) was limited, the robot's links did not violate their respective virtual walls (distances $d_{6,C_1}/d_{4,C_2}$). This holds true, even during excessive physical interaction forces ($\mathbf{w}^{0,6}_{C_{1,6}}$ between $16.2-18$ s and $23-26.2$ s; $\mathbf{w}^{0,4}_{C_{2,4}}$ between $\sim 20-22$ s).

B. Approach 2: Flow limiting

This subsection will show the benefits of approach 2 by referring to Figure 4. When the gripper released the fixture during the accidental phase ($\sim$ 14.5 s in highlighted green area)., a similar behavior to the previous experiment (subsection III-A) could be seen: while entering the activation

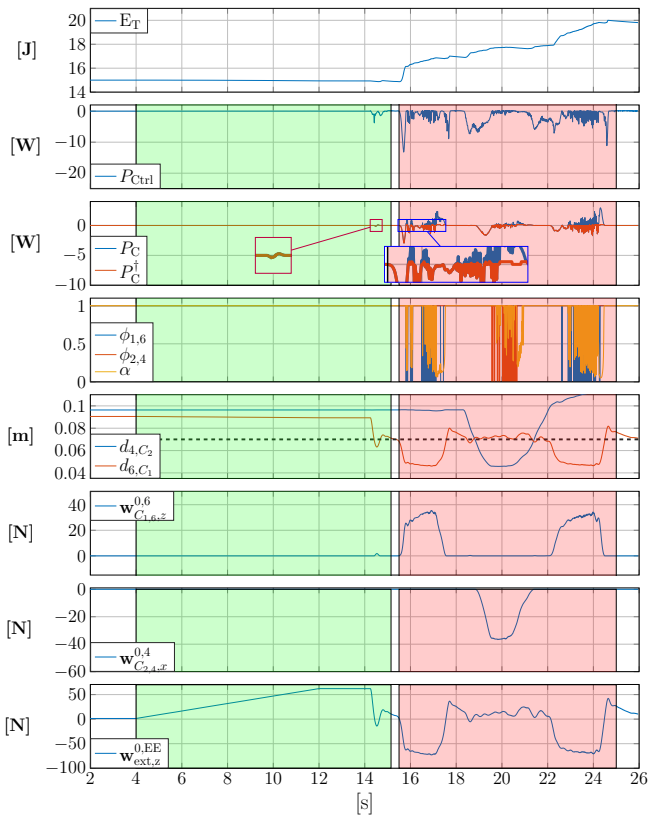

Fig. 4. Observable quantities of approach 2: energy tank E_T; energy flow P_{Ctrl}; unrestricted and by α, $\phi_{1,6}$, and $\phi_{2,4}$ restricted energy flow P_C; repelling wrenches $\mathbf{w}^{0,6}_{C_{1,6},z}$ and $\mathbf{w}^{0,4}_{C_{2,4},x}$ of virtual walls C_1 and C_2 along their repelling direction; external wrench along the TCP's z-axis, $\mathbf{w}^{0,EE}_{ext,z}$.

distance energy was dissipated ($P_{\text{Ctrl}} < 0$) and while exiting the activation distance, energy was produced ($P_{\text{Ctrl}} > 0$). However, P_{Ctrl} did not reach the energy flow limit during the $\overline{P}_{\text{Ctrl}}$ (magnified in the purple window). During the pHRI-phase (highlighted in red), link 6 and 4 were manually pushed into their respective virtual walls C_1 and C_2 (C_1 between $15.7 - 17.7$ s and $22 - 24.5$ s for link 6; C_2 between $\sim 19 - 21$ s for link 4). As already observed in subsection III-A, during the external disturbance, the energy was virtually dissipated ($P < 0$ at port $(\boldsymbol{\tau}_C, \dot{\mathbf{q}})$) when entering the activation distance (dashed line). When the externally applied wrenches $\mathbf{w}^{0,6}_{C_{1,6}}$/$\mathbf{w}^{0,4}_{C_{2,4}}$ reached their maximum, a similar behavior as described in subsection III-A occurred: The energy flow at port $(\boldsymbol{\tau}_C, \dot{\mathbf{q}})$ fluctuated between its passive and non-passive direction, due to minor fluctuation of the externally applied wrench. However, for approach 2, the passivity check did not utilize the concept of energy tanks (virtually stored energy). Instead, P_C was limited through the scaling factor α (equation (15)) and the individual decoupling terms $\phi_{1,6}$ and $\phi_{2,4}$ for constraint 1,2 and joint 4 and 6, respectively (equation (18)). The blue magnified window shows the response of $P_C^\dagger$ when link 6 is subjected to C_1. It can be observed how $P_C^\dagger$ changed between $\overline{P}_C$ and 0. In the event that the limited positive energy flow αP_C would have led to an overall active system ($P_{\text{Ctrl}} > 0$), $\phi_{1,6}$ becomes 0, decoupling $P_{C_{1,6}}$ from the energy flow at $(\boldsymbol{\tau}_C, \dot{\mathbf{q}})$ (equation (18)). Hence, $P_{\text{Ctrl}} \leq 0$ and the overall system was kept passive. Even when subjected to excessive forces, approach 2 did not penetrate their respective virtual walls.

IV. Summary & Discussion

In this paper, we proposed and compared two approaches to ensure the passivity of an energy-aware Cartesian Impedance controller which is able to handle virtual Cartesian workspace restrictions, called virtual walls. The paper showed the concept its applicability in three steps.
Firstly, the energetic behavior of all control actions were analyzed and their influence on the overall passivity of the system were shown. It was found that that virtual wall initially dissipates the energy of an entering link and injects energy as the link exits the virtual wall.
Secondly, two approaches to handle non-passive actions were presented: 1) Approach 1 employed an enhanced energy tank method to guarantee passivity, while restricting the energy flow from the tank. The energy tank was designed to efficiently collaborate with a second energy tank, which was needed to ensure passivity of the Cartesian impedance controller. 2) Approach 2 observed and limited the overall energy flow of the controller, without utilizing an additional energy tank. In case of non-passive control actions, the approach decoupled individual energy flows.
Thirdly, both approaches were evaluated based on a proof-of-concept component extraction experiment. During the experiment, multiple pHRI-scenarios were tested. Even when subjected to significant external forces, both approaches did not violate the virtual walls and the robotic system remained passive.
When analyzing the two approaches, each presented its own challenges. For approach 1, suitable upper and lower bounds for the energy tank have to be selected. The determination of these values is non-trivial due to the unpredictability of the robot's interactions with the virtual walls in terms of their intensity, timing, and energy flow behavior. For approach 2, the primary challenge is the increased complexity involved in monitoring and decoupling the energy flows of multiple constraints and links. For both approaches, it was noticed that the energy flow associated with the virtual wall exhibited fluctuations when it was maintained at maximum penetration. These fluctuations were evident in the restrictive scaling factor of the energy flow as well. Due to the decoupling term in approach 2, minor oscillation occured when link 6 was encountered the virtual wall.

V. Future Work

While this paper focused on virtual walls, future work will extend this concept to guarantee the passivity of joint space constraints, e.g., joint limits [12]. Hereby, similar concepts can be employed. In our control approaches, we did not establish any direct interaction between the controller parts of the task and the virtual walls. In future research, we plan to explore the integration of conflict detection between the task and virtual walls [23] into the scaling of the task stiffness.

REFERENCES

[1] E. Commission, "Circular Economy Action Plan," European Commission, Tech. Rep., 2015.

[2] European Environment Agency, "Recycling industry can boost the European economy," p. 2020, 2020. [Online]. Available: https://www.eea.europa.eu/highlights/recycling-industry-can-boost-the

[3] T. Tolio, A. Bernard, M. Colledani, S. Kara, G. Seliger, J. Duflou, O. Battaia, and S. Takata, "Design, management and control of demanufacturing and remanufacturing systems," *CIRP Ann. - Manuf. Technol.*, vol. 66, no. 2, pp. 585–609, 2017.

[4] K. Elo and E. Sundin, "Automatic dismantling challenges in the structural design of LCD TVs," *Procedia CIRP*, vol. 15, pp. 251–256, 2014.

[5] S. Hjorth and D. Chrysostomou, "Humanrobot collaboration in industrial environments: A literature review on non-destructive disassembly," *Robotics and Computer-Integrated Manufacturing*, vol. 73, p. 102208, 2022.

[6] R. Li, C. Ji, Q. Liu, Z. Zhou, D. T. Pham, J. Huang, Y. Tan, M. Qu, Y. Wang, M. Kerin, K. Jiang, and S. Su, "Unfastening of Hexagonal Headed Screws by a Collaborative Robot," *IEEE Trans. Autom. Sci. Eng.*, pp. 1–14, 2020.

[7] J. Huang, D. T. Pham, R. Li, M. Qu, Y. Wang, M. Kerin, S. Su, C. Ji, O. Mahomed, R. Khalil, D. Stockton, W. Xu, Q. Liu, and Z. Zhou, "An experimental human-robot collaborative disassembly cell," *Computers & Industrial Engineering*, vol. 155, p. 107189, 2021.

[8] J. Huang, D. T. Pham, Y. Wang, M. Qu, C. Ji, S. Su, W. Xu, Q. Liu, and Z. Zhou, "A case study in humanrobot collaboration in the disassembly of press-fitted components," *Proceedings of the Institution of Mechanical Engineers, Part B: Journal of Engineering Manufacture*, vol. 234, no. 3, pp. 654–664, 2020.

[9] J. Lachner, F. Allmendinger, E. Hobert, N. Hogan, and S. Stramigioli, "Energy budgets for coordinate invariant robot control in physical humanrobot interaction," *The International Journal of Robotics Research*, vol. 40, no. 8-9, pp. 968–985, 2021.

[10] S. Stramigioli, "Energy-aware robotics," in *Mathematical Control Theory I*, M. K. Camlibel, A. A. Julius, R. Pasumarthy, and J. M. Scherpen, Eds. Cham: Springer International Publishing, 2015, pp. 37–50.

[11] J. D. Muoz Osorio, F. Allmendinger, M. D. Fiore, U. E. Zimmermann, and T. Ortmaier, "Physical Human-Robot Interaction under Joint and Cartesian Constraints," *ICRA*, pp. 185–191, 2019.

[12] S. Hjorth, J. Lachner, S. Stramigioli, O. Madsen, and D. Chrysostomou, "An energy-based approach for the integration of collaborative redundant robots in restricted work environments," in *2020 IEEE/RSJ International Conference on Intelligent Robots and Systems (IROS)*. IEEE, 2020, pp. 7152–7158.

[13] A. M. Zanchettin, B. Lacevic, and P. Rocco, "Passivity-based control of robotic manipulators for safe cooperation with humans," *International Journal of Control*, vol. 88, no. 2, pp. 429–439, 2015. [Online]. Available: https://doi.org/10.1080/00207179.2014.956338

[14] Y. Zhang, S. Li, J. Zou, and A. H. Khan, "A passivity-based approach for kinematic control of manipulators with constraints," *IEEE Transactions on Industrial Informatics*, vol. 16, pp. 3029–3038, 2020.

[15] J. M. S. Ducaju, B. Olofsson, A. Robertsson, and R. Johansson, "Robot cartesian compliance variation for safe kinesthetic teaching using safety control barrier functions," *2022 IEEE 18th International Conference on Automation Science and Engineering (CASE)*, pp. 2259–2266, 2022.

[16] V. Kurtz, P. M. Wensing, and H. Lin, "Control barrier functions for singularity avoidance in passivity-based manipulator control," in *2021 60th IEEE Conference on Decision and Control (CDC)*. IEEE, 2021, pp. 6125–6130.

[17] M. Rauscher, M. Kimmel, and S. Hirche, "Constrained Robot Control Using Control Barrier Functions," *IEEE IROS*, pp. 279–285, 2016.

[18] J. Lachner, F. Allmendinger, S. Stramigioli, and N. Hogan, "Shaping impedances to comply with constrained task dynamics," *IEEE Transactions on Robotics*, 2022.

[19] S. Hjorth, E. Lamon, D. Chrysostomou, and A. Ajoudani, "Design of an energy-aware cartesian impedance controller for collaborative disassembly," 2023.

[20] R. Murray, Z. Li, S. Sastry, and S. Sastry, *A Mathematical Introduction to Robotic Manipulation*. Taylor & Francis, 1994.

[21] J. Lachner, "A geometric approach to robotic manipulation in physical human-robot interaction," Ph.D. dissertation, University of Twente, Netherlands, Jul. 2022.

[22] V. Duindam, A. Macchelli, S. Stramigioli, and H. Bruyninckx, *Modeling and Control of Complex Physical Systems*. Springer Berlin Heidelberg, 2009.

[23] V. Schettino, M. Fiore, C. Pecorella, F. Ficuciello, F. Allmendinger, J. Lachner, S. Stramigioli, and B. Siciliano, "Geometrical interpretation and detection of multiple task conflicts using a coordinate invariant index," in *2020 IEEE/RSJ International Conference on Intelligent Robots and Systems, IROS 2020*, Feb. 2021, pp. 6613–6618.